GEOPHYSICAL RESEARCH LETTERS, VOL. 37, L10602, doi:10.1029/2010GL042657, 2010

An almost-free barotropic mode in the Australian-Antarctic Basin

Wilbert Weijer[1]

Received 25 January 2010; revised 19 April 2010; accepted 20 April 2010; published 19 May 2010.

[1] The Australian-Antarctic Basin (AAB) is known for its high levels of intraseasonal variability; sea-surface height variability exceeds background values by factors of 2 over thousands of kilometers. This paper addresses the hypothesis that this variability is caused by trapping of barotropic energy by the basin geometry. Analysis of a multi-year integration of a shallow-water model shows that the variability is dominated by a single, large-scale statistical mode that is highly coherent over the entire AAB. The flow associated with this mode is northwestward along the Southeast Indian Ridge, southward in the Kerguelen Abyssal Plain, and eastward in the southern AAB. The mode is interpreted as an almost-free topographically trapped mode, as it is confined by contours of potential vorticity that almost entirely enclose the AAB. The apex of the Wilkes Abyssal Plain represents the strongest barrier to the modal circulation: here velocities are strongest, making it a key area for dissipation of kinetic energy through bottom friction and eddy viscosity. **Citation:** Weijer, W. (2010), An almost-free barotropic mode in the Australian-Antarctic Basin, *Geophys. Res. Lett.*, *37*, L10602, doi:10.1029/2010GL042657.

1. Introduction

[2] Wind forcing is among the main drivers of the ocean circulation. It is believed to be an important source of energy for turbulence-driven mixing in the abyss and, as such, essential for maintaining a vigorous overturning circulation [e.g., *Wunsch and Ferrari*, 2004]. Identifying how and where this energy is dissipated is thus important for understanding the dynamics of the global-scale ocean circulation and its role in climate.

[3] The Southern Ocean has been identified as an important region for the energetics of the global circulation [e.g., *Wunsch*, 1998]. Here, the vigorous wind forcing and weak stratification allow for an energetic circulation that is strongly controlled by bathymetry. In fact, analysis of altimeter data have identified several regions in the Southern Ocean where sea-surface height (SSH) variability is exceptionally strong [e.g., *Chao and Fu*, 1995]. One of these areas is the Australian-Antarctic Basin (AAB, Figure 1). Located between Australia and Antarctica, it accommodates the Kerguelen Abyssal Plain (KAP) and the Wilkes Abyssal Plain (WAP), as well as an extensive mid-ocean ridge system known as the Southeast Indian Ridge (SIR). This ridge consists of eastern (ESIR) and western (WSIR) segments that are offset by the WAP.

[4] Studies addressing the anomalous SSH variability in the AAB suggest a link with the local bathymetry [e.g., *Chao and Fu*, 1995; *Fukumori et al.*, 1998; *Ponte and Gaspar*, 1999; *Webb and De Cuevas*, 2002; *Fu*, 2003; *Vivier et al.*, 2005; *Weijer and Gille*, 2005a; *Weijer et al.*, 2009]. In particular, *Webb and De Cuevas* [2002] (hereafter WD02) concluded that the enhanced variability reflects the resonant excitation of a topographically trapped mode. However, they found this mode to decay too fast to be consistent with frictional spin-down [e.g., *Fu*, 2003; *Weijer et al.*, 2009]. Instead, they suggested that energy may be leaking from the mode at the apex ('mouth') of the WAP, and escape along the northern flank of the WSIR. This conclusion was supported by *Vivier et al.* [2005], who found that SSH variability in the AAB increased in their model when they turned off the inertia term, apparently at the expense of the variability on the WSIR.

[5] *Weijer et al.* [2009] (hereafter WGV) have shown that at least part of the SSH variability can indeed be attributed to the resonant excitation of free topographically trapped modes. These modes represent balanced circulation patterns along closed contours of potential vorticity (defined as f/H, where f is the Coriolis parameter and H the local water depth) that surround in particular the WAP and the crest of the WSIR. However, the two dominant modes were found to explain only a fraction of the variance, leaving the main characteristics of the anomalous SSH variability unaccounted for. In addition, the slow, frictional decay of these modes is inconsistent with the rapid decay found by WD02.

[6] In this paper we study the dynamics of the variability in the AAB that was unexplained by WGV. The analysis suggests that the specific distribution of f/H in the AAB gives rise to a so-called almost-free mode response to wind stress forcing [*Hughes et al.*, 1999]. This response is characterized by i) highly coherent motion over the entire AAB; ii) flow aligned mostly along contours of f/H surrounding the basin; iii) a key region where the flow has to jump contours of f/H; leading to iv) relatively rapid decay compared with the frictional spin-down of purely free modes. A detailed analysis of the energetics shows that the modal response is a very important aspect of the regional circulation as it funnels energy towards the apex of the WAP for dissipation, and for transfer to non-modal flow.

2. Method

[7] Since the anomalous variability in the AAB is thought to be dominantly barotropic, a 1-layer shallow-water (SW) model is used to study its most important characteristics. The computational domain ranges from 45° to 185° east longitude, and from −70° to 0° latitude, encompassing the South Indian Ocean and the Indian sector of the Southern Ocean. Diagnostic focus is on a subdomain that ranges from 68° to 145° east longitude and −65° to −30° latitude, covering the greater AAB. Forcing is provided by daily-averaged wind stress, based on the 10 m wind velocity of *Milliff et al.* [2004]. The model was integrated for 1003 days, starting August 1,

[1]Los Alamos National Laboratory, Los Alamos, New Mexico, USA.

0094-8276/10/2010GL042657

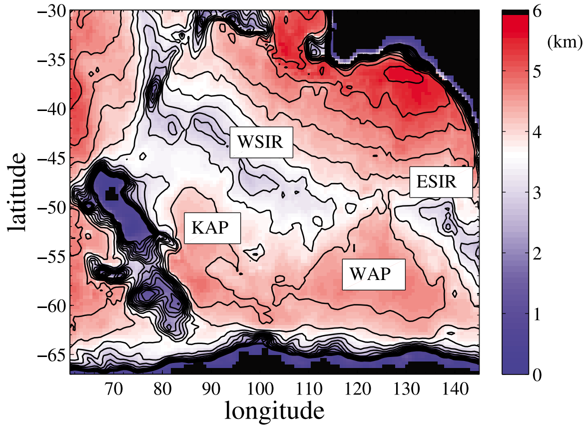

Figure 1. Bathymetry of the Australian-Antarctic Basin. ESIR and WSIR: Eastern and western segments of the Southeast Indian Ridge; WAP: Wilkes Abyssal Plain; KAP: Kerguelen Abyssal Plain. Black contours are isolines of the base-10 logarithm of f/H (scaled by -1 m^{-1} s^{-1}), plotted for the interval [−9.0, −7.0] with step 0.5.

1999, and daily averages of the dynamical fields η, u and v (SSH, and the zonal and meridional velocity components, respectively) were saved. In order to focus on the variability that could not be explained by free modes, we repeated the normal-mode analysis of WGV to determine as many modes as possible, and filtered out their signal from the dynamical fields. Subsequent analyses described below are based on these residual fields. In some areas, specifically the WAP, the free modes account for up to 50% of the SSH variability. See section 1 of the auxiliary material for a more detailed description of the modeling approach.[1]

3. A Topographically Trapped Mode in the AAB

3.1. Spatial Structure

[8] In order to determine the spatial structure of the variability we first perform an Empirical Orthogonal Function (EOF) analysis on the daily-averaged SSH fields, box-averaged onto a coarser grid of 2° × 2° resolution. The analysis is dominated by the first EOF, which accounts for 46.6% of the SSH variance (section 2.1 of the auxiliary material). The pattern clearly resembles the dominant EOFs of SSH variability determined by WD02 and *Fu* [2003]. Additional statistical analyses (section 2.2 of the auxiliary material) show that the EOF represents variability that is highly coherent throughout the basin: local SSH time series are significantly coherent with its amplitude time series (principal component) $\Gamma_1(t)$ for essentially all frequencies below 1/30 cpd; time lags are a few days at most.

[9] The principal component Γ_1 is used to construct a composite pattern of the SSH and velocity fields that we will refer to as the statistical mode: $\mathbf{u}_m = \overline{\mathbf{u}\Gamma_1}$, where $\mathbf{u} = (u, v, \eta)$, and the overline denotes the average over the 1003-day time series (Figure 2). The composite pattern of SSH is equivalent to the EOF except for the higher spatial resolution; it shows positive loadings in the entire AAB. In fact, the pattern is clearly enclosed by the blue and red contours of potential vorticity (representing values of $-3.2 \cdot 10^{-8}$ and $-2.5 \cdot 10^{-8}$m^{-1} s^{-1}, respectively), that nearly bound the basin. The circulation associated with this pattern displays intense northwestward transport along the northern flank of the WSIR and the southern flank of the ESIR; broad southward flows in the basin between the WSIR and the Kerguelen Plateau; and eastward drifts in the southern part of the basin.

[10] In summary, almost half of the variability in the AAB is captured by a single EOF. The facts that the associated variability is i) stationary and highly coherent, and ii) strongly linked to bathymetry, support the interpretation that it is caused by a topographically trapped mode. In the remainder of this paper we assume that the statistical mode represents such a dynamical object.

3.2. Decay and Energetics

[11] To study the decay of the topographically trapped mode, we use the velocity field of the statistical mode depicted in Figure 2 to initialize a transient, unforced integration of the SW model. The model is run for 10 days. Projection of the composite velocity patterns on the daily averaged velocity fields yields the two projection time series γ^u and γ^v for zonal and meridional velocity, respectively. These time series record a rapid decay, and reach the $1/e$ threshold after about 5 or 6 days (section 3 of the auxiliary material). This decay rate is much faster than what can be expected from frictional spin-down. In fact, similar rapid decay was deduced by WD02, who suggested that the mode may lose energy to non-modal circulation.

[12] In order to address this hypothesis, we study the energetics of the mode in the forced and unforced simulations. We decompose the velocity field in the modal contribution $\mathbf{u}_m$ and a residual $\mathbf{u}_r = \mathbf{u} - \mathbf{u}_m$ at each time step. Based

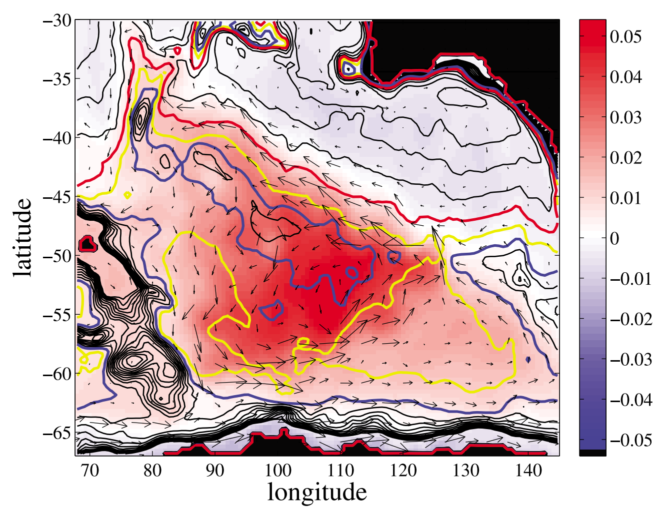

Figure 2. Composite fields of SSH (shading; in meters) and velocity (arrows), obtained by regressing the daily-averaged fields on Γ_1. Velocity vectors denote box-averaged values over squares of 5 × 5 grid points. Maximum values are of the order of 0.02 m s^{-1}. Contours represent isolines of f/H as in Figure 1; blue, yellow and red contours represent the values -3.2×10^{-8}, -2.8×10^{-8} and -2.5×10^{-8} m s^{-1}, respectively.

[1]Auxiliary materials are available in the HTML. doi:10.1029/2010GL042657.

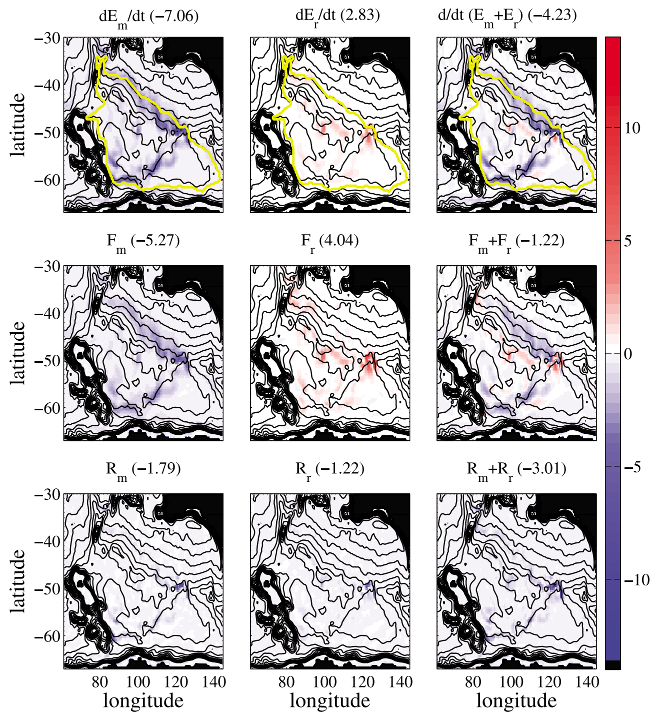

Figure 3. Terms in the balance of kinetic energy equations (1a) and (1b) for the unforced, decaying integration (in mW m^{-2}). Numbers in brackets denote integrals (in GW) over the modal area. This area is indicated by the yellow line in the top left plot. Work done by wind stress is zero. See text for details.

on this decomposition, we can determine a balance for the kinetic energy of the actual mode, $E_m = \frac{1}{2}\rho_0 H|\mathbf{u}_m|^2$, and of the residual, $E_r = \frac{1}{2}\rho_0 H|\mathbf{u}_r|^2$:

$$\frac{dE_m}{dt} = F_m + R_m + W_m \tag{1a}$$

$$\frac{dE_r}{dt} = F_r + R_r + W_r \tag{1b}$$

Input of kinetic energy by wind stress forcing is indicated by W, local dissipation due to friction by R, while the residual F represents other mechanisms of energy transfer. These mechanisms include work done by the Coriolis and pressure gradient forces that either transfer energy between E_m and E_r, or remove energy locally to be deposited elsewhere. See section 4 of the auxiliary material for a detailed discussion of these terms.

[13] Figure 3 shows the terms in the kinetic energy balance equations (1a) and (1b), averaged over the first 6 days of the unforced, decaying integration. Energy input by wind stress is zero. Terms in brackets denote the values integrated over the modal area, defined as the region where the amplitude of the dominant EOF exceeds 1/6th of its maximum value (indicated by the yellow contour in the top plots).

[14] The area-integrated values show that the mode loses 25% (1.79 GW) of its energy locally to frictional processes. This energy loss is concentrated at the apex of the WAP. About 17% (1.22 GW) is exported from the modal area altogether by energy fluxes. The largest part (57%; 4.04 GW), however, is transferred to the residual circulation within the modal area. Although the mode loses most of its energy over the northern flank of the WSIR and along the northwestern edge of the WAP, the residual circulation picks up most of its energy at the apex of the WAP. A flux of energy is implied by these sources and sinks, and evidently the apex of the WAP is an area of energy flux convergence. A substantial part of the energy gained by the residual circulation is immediately dissipated by friction.

[15] Analysis of the energetics of the 1003-day forced run is fully consistent with this picture (Figure 4). No less than 21% (0.37 GW, the average over the 1003 days of integration) of the energy input by the wind stress is used to energize the mode. About 38% of this energy (0.14 GW) is dissipated through friction, most of which at the apex of the WAP. As was the case for the unforced simulation, there is a strong localized source of energy for the non-modal circulation at the apex of the WAP, and it is likely that a substantial fraction of this energy is derived from the mode. These results suggest that also in the wind forced case there is a significant transfer of energy from the mode to the residual circulation, and that the prime location for this transfer is the apex of the WAP.

4. Summary and Discussion

[16] In this paper we studied the nature of the high SSH variability in the AAB. The analysis suggests that the variability identified by WD02 and *Fu* [2003] is indeed caused by the resonant excitation of a topograpically trapped mode. It is found that similar variability i) can be reproduced by a barotropic SW model forced with realistic wind stress; ii) is

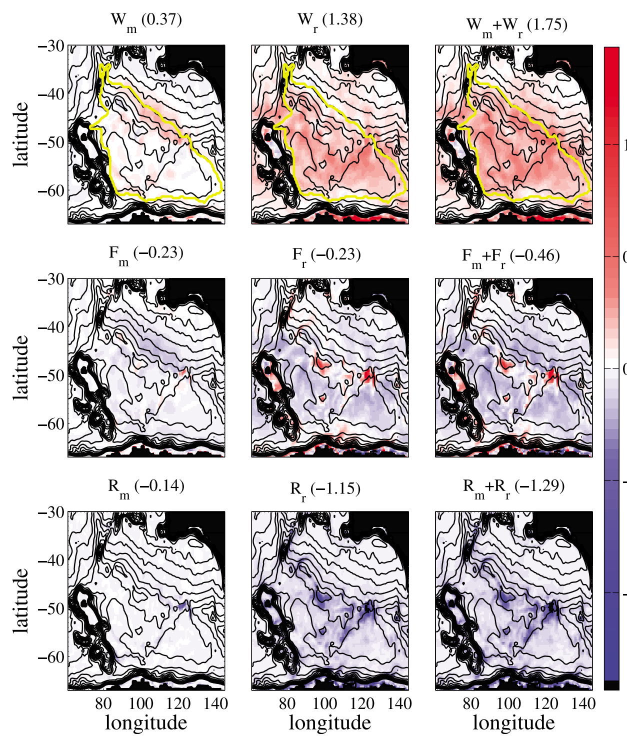

Figure 4. As Figure 3, but now for the forced integration. The tendency terms are negligibly small, and incorporated in F for completeness. Top plots now show work done by wind stress.

clearly confined by specific contours of potential vorticity that almost completely enclose the AAB; and iii) has a high spatial coherence for all time scales exceeding a month, displaying a negligible time lag of ±2 days over the extent of the basin.

[17] What is the nature of this mode? Despite a large number of normal-mode calculations, WGV found no free modes that are consistent with the statistical mode determined in this study. Although it is impossible to determine *all* modes, the analysis usually determines the 'strongest' modes with ease, and it seems unlikely that the current mode was simply missed.

[18] A more likely interpretation is that the statistical mode does not reflect a free mode in the strictest sense of the word: a dynamical object that fully preserves its spatial structure while evolving in time. Instead, it shows characteristics of an *almost-free* mode, a concept introduced by *Hughes et al.* [1999] to explain a band of high SSH variability around Antarctica called the Southern Mode. As is the case there, the AAB is surrounded by contours of f/H that are almost continuous, if not for a few choke points, most notably the apex of the WAP. *Hughes et al.* [1999] argued that a continuous circulation can only exist by the grace of a vorticity source at the choke points that allows the flow to jump contours of f/H. In the absence of forcing (and significant friction), the mode can only negotiate the jump in f/H by a local change in relative vorticity, causing the mode to lose its coherence and hence its true modal character. Indeed, in the decaying simulation the advection of potential vorticity attains its maximum amplitudes there (not shown). And although friction does its part, there is a substantial residual that locally generates relative vorticity.

[19] It is clear from this study that the topographically trapped mode has significant impact on the energetics of the AAB. It receives a substantial amount of energy from the wind, but instead of expending it on friction (as would be the case for the free modes described in WGV), most of the energy is funneled to the apex of the WAP to power a residual, non-modal circulation. This result supports the conclusion by WD02 and *Vivier et al.* [2005], who suggested that energy may be extracted from the mode by waves emanating from the apex of the WAP, and propagating along the northern flank of the WSIR. The mode plays hence an important role in redistributing energy over large distances [e.g., *Weijer and Gille*, 2005b], and points to the apex of the WAP as a potential location of enhanced dissipative mixing.

[20] **Acknowledgments.** This research was supported by the Climate Change Prediction Program of the U.S. Department of Energy Office of Science and by NSF-OCE award 0928473. Los Alamos National Laboratory is operated by the Los Alamos National Security, LLC for the National Nuclear Security Administration of the U.S. Department of Energy under contract DE-AC52-06NA25396. Wind stress curl data were provided by the Data Support Section of the Computational and Information Systems Laboratory at the National Center for Atmospheric Research. Constructive comments by Matthew Hecht and two anonymous reviewers are gratefully acknowledged.

References

Chao, Y., and L.-L. Fu (1995), A comparison between the TOPEX/POSEIDEON data and a global ocean general circulation model during 1992–1993, *J. Geophys. Res.*, *100*, 24,965–24,976.

Fu, L.-L. (2003), Wind-forced intraseasonal sea level variability of the extratropical oceans, *J. Phys. Oceanogr.*, *33*, 436–449.

Fukumori, I., R. Raghunath, and L.-L. Fu (1998), Nature of global large-scale sea level variability in relation to atmospheric forcing: A modeling study, *J. Geophys. Res.*, *103*, 5493–5512.

Hughes, C. W., M. P. Meredith, and K. J. Heywood (1999), Wind-driven transport fluctuations through Drake Passage: A southern mode, *J. Phys. Oceanogr.*, *29*, 1971–1992.

Milliff, R. F., J. Morzel, D. B. Chelton, and M. H. Freilich (2004), Wind stress curl and wind stress divergence biases from rain effects on QSCAT surface wind retrievals, *J. Atmos. Oceanic Technol.*, *21*, 1216–1231.

Ponte, R. M., and P. Gaspar (1999), Regional analysis of the inverted barometer effect over the global ocean using TOPEX/POSEIDON data and model results, *J. Geophys. Res.*, *104*, 15,587–15,601.

Vivier, F., K. A. Kelly, and M. Harismendy (2005), Causes of large-scale sea level variations in the Southern Ocean: Analyses of sea level and a barotropic model, *J. Geophys. Res.*, *110*, C09014, doi:10.1029/2004JC002773.

Webb, D. J., and B. A. De Cuevas (2002), An ocean resonance in the Indian sector of the Southern Ocean, *Geophys. Res. Lett.*, *29*(14), 1664, doi:10.1029/2002GL015270.

Weijer, W., and S. T. Gille (2005a), Adjustment of the Southern Ocean to wind forcing on synoptic time scales, *J. Phys. Oceanogr.*, *35*, 2076–2089.

Weijer, W., and S. T. Gille (2005b), Energetics of wind-driven barotropic variability in the Southern Ocean, *J. Mar. Res.*, *63*, 1101–1125.

Weijer, W., S. T. Gille, and F. Vivier (2009), Modal decay in the Australia-Antarctic Basin, *J. Phys. Oceanogr.*, *39*, 2893–2909.

Wunsch, C. (1998), The work done by the wind on the oceanic general circulation, *J. Phys. Oceanogr.*, *28*, 2332–2340.

Wunsch, C., and R. Ferrari (2004), Vertical mixing, energy, and the general circulation of the oceans, *Ann. Rev. Fluid Mech.*, *36*, 281–314.

W. Weijer, CCS-2, MS B296, Los Alamos National Laboratory, Los Alamos, NM 87545, USA. (wilbert@lanl.gov)